

# Recent Advances for Improving the Accuracy, Transferability, and Efficiency of Reactive Force Fields

Itai Leven, Hongxia Hao, Songchen Tan, Xingyi Guan, Katheryn A. Penrod, Dooman Akbarian, Benjamin Evangelisti, Md Jamil Hossain, Md Mahbubul Islam, Jason P. Koski, Stan Moore, Hasan Metin Aktulga, Adri C. T. van Duin, and Teresa Head-Gordon\*



Cite This: *J. Chem. Theory Comput.* 2021, 17, 3237–3251



Read Online

ACCESS |

Metrics & More

Article Recommendations

**ABSTRACT:** Reactive force fields provide an affordable model for simulating chemical reactions at a fraction of the cost of quantum mechanical approaches. However, classically accounting for chemical reactivity often comes at the expense of accuracy and transferability, while computational cost is still large relative to nonreactive force fields. In this Perspective, we summarize recent efforts for improving the performance of reactive force fields in these three areas with a focus on the ReaxFF theoretical model. To improve accuracy, we describe recent reformulations of charge equilibration schemes to overcome unphysical long-range charge transfer, new ReaxFF models that account for explicit electrons, and corrections for energy conservation issues of the ReaxFF model. To enhance transferability we also highlight new advances to include explicit treatment of electrons in the ReaxFF and hybrid nonreactive/reactive simulations that make it possible to model charge transfer, redox chemistry, and large systems such as reverse micelles within the framework of a reactive force field. To address the computational cost, we review recent work in extended Lagrangian schemes and matrix preconditioners for accelerating the charge equilibration method component of ReaxFF and improvements in its software performance in LAMMPS.



## INTRODUCTION

Reactive force fields offer an efficient model for simulating chemical reactions within the framework of a classical description, enabling the simulation of time and length scales that are orders of magnitude higher than purely quantum mechanical approaches. One of the more popular reactive force fields is ReaxFF, which employs a distance-dependent formalism to bond-order changes for chemical reactivity within a fully classical model.<sup>11</sup> ReaxFF has been applied to a wide range of research fields including surface science,<sup>40,47,49</sup> energetic materials,<sup>14,31,45</sup> electrolysis,<sup>34,46,59</sup> and biochemistry.<sup>24,32,48</sup>

A key feature of ReaxFF is its ability to account for charge rearrangement as bonds are broken and formed. This has been historically achieved through the electronegativity equalization method (EEM) originally proposed by Mortier et al. over three decades ago<sup>3,4</sup> and later refined by Rappé et al. and termed the charge equilibration method (CEM) or charge equalization (QEeq).<sup>7</sup> However, the simplifications associated with classically accounting for the electronic degrees of freedom using EEM in ReaxFF has notable shortcomings in some applications<sup>33,56</sup> including unphysical long-range charge transfer, noninteger molecular charge at large separations, lack of out-of-plane polarization, lack of energy conservation, poor parametrization, and lack of transferability. In addition, while ReaxFF offers an

affordable method with respect to quantum chemistry, it is still substantially more expensive than nonreactive force fields and therefore increasing its efficiency is highly desirable.<sup>21,22,61</sup> This computational cost arises in part from the EEM methods that require solving a set of linear equations self-consistently, in which previous work has shown that EEM can account for ~80% of the computational time for ReaxFF applied to large systems and tight convergence tolerance.<sup>22,54</sup>

Here we consider recent advancements that have been developed in order to address some of these issues. Methods such as the split-charge equilibration (SQE)<sup>17</sup> and the atom condensed Kohn–Sham DFT approximated to second order (ACKS2)<sup>25</sup> were designed to impede unphysical long-range charge transfer, and new reactive force field models that account for electrons and electron density more explicitly have improved overall accuracy, including the coarse-grained electron model (C-GeM)<sup>54,60</sup> and explicit electron ReaxFF (eReaxFF) model,<sup>35</sup>

Received: February 1, 2021

Published: May 10, 2021



which are also designed to be more transferable. We illustrate this progress in applications including Ag nanoclusters,<sup>57</sup> hydrocarbons,<sup>35</sup> lithium ion batteries,<sup>36</sup> electrical breakdown of polyethylene,<sup>66</sup> and water in different condensed phase environments.<sup>54,60</sup> We also consider the benefit derived from hybrid models in which C-GeM is embedded in a classical electrostatic force field to describe proton hopping mechanisms in the water pool of reverse micelles. Finally, we review the recent efforts that have been devoted to reducing the computational cost of EEM, including matrix preconditioners<sup>21,50,61</sup> and extended Lagrangian schemes,<sup>54,64</sup> which largely have fully eliminated the cost of the self-consistent field (SCF) altogether, as well as better optimized performance of these methods in community codes such as large-scale atomic/molecular massively parallel simulator (LAMMPS).

## BOND ORDER REACTIVE FORCE FIELDS

Bond order reactive force fields are targeted toward describing electronic rearrangements involving chemical reactivity within classical models. Some of the early incarnations of reactive force fields include the Tersoff,<sup>5</sup> REBO,<sup>6</sup> and AIREBO<sup>13</sup> potentials that were developed to describe the different phases of hydrocarbons within one theoretical framework. Subsequently models such as the ReaxFF<sup>11</sup> and COMB<sup>18</sup> potentials have expanded the chemical space for reactivity beyond just hydrocarbons, and advanced their applicability by combining the bond order terms with charge equilibration methods<sup>4,7</sup> to describe the charge rearrangement as bonds break and form. Here we review the ReaxFF method specifically to illustrate the ideas behind bond order reactive force fields.

In ReaxFF, the total energy is decomposed into various partial energy contributions, similar to nonreactive force fields. Unlike the nonreactive force field counterparts, which use fixed bond connectivity, ReaxFF computes bond orders as a function of interatomic distance. These bond orders are then incorporated into flexible bonded terms that contribute to the total ReaxFF energy and forces. In addition, ReaxFF computes nonbonded interactions using shielded Coulomb and van der Waals (vdW) potentials.

More specifically, the partial energy contributions to the ReaxFF total energy are as follows:

$$\begin{aligned} E_{\text{ReaxFF}} = & E_{\text{bond}} + E_{\text{over}} + E_{\text{under}} + E_{\text{lp}} + E_{\text{val}} + E_{\text{tors}} \\ & + E_{\text{vdW}} + E_{\text{Coul}} + E_{\text{specific}} \end{aligned} \quad (1)$$

The first six terms on the right-hand side of eq 1 correspond to the flexible bond-order-dependent energy terms. The first of these terms,  $E_{\text{bond}}$ , captures the energy from the breaking and formation of chemical bonds in the system. To compute the second, third, and fourth terms, the ReaxFF bond orders are compared to the valency expected based on atom type. The second term,  $E_{\text{over}}$ , is an energetic penalty applied to over-coordinated atoms. Analogously,  $E_{\text{under}}$  is an energetic stabilization applied to undercoordinated atoms. The fourth term,  $E_{\text{lp}}$ , represents the energy from lone-pair electrons. The fifth and sixth terms,  $E_{\text{val}}$  and  $E_{\text{tors}}$ , describe the three-body valence angle strain and the four-body torsional angle strain, respectively. These bonded terms are followed by the nonbonded vdW and Coulombic contributions ( $E_{\text{vdW}}$  and  $E_{\text{Coul}}$ ), which are computed for all atom pairs regardless of connectivity. The final term represents a force-field-specific parameter used to account for additional energy contributions for a particular

system of interest (i.e., conjugation, hydrogen bonding, C2 corrections, system-specific torsions). We review the functional forms of some of these partial energy contributions, and they are also described in more detail in previous publications.<sup>11,19,42</sup>

In ReaxFF, the bond order is calculated from interatomic distances using the following continuous equation:

$$\begin{aligned} \text{BO}_{ij} = & \text{BO}_{ij}^{\sigma} + \text{BO}_{ij}^{\pi} + \text{BO}_{ij}^{\pi\pi} \\ = & \exp\left[p_{\text{bo1}}\left(\frac{r_{ij}}{r_0^{\sigma}}\right)^{p_{\text{bo1}}}\right] + \exp\left[p_{\text{bo3}}\left(\frac{r_{ij}}{r_0^{\pi}}\right)^{p_{\text{bo3}}}\right] \\ & + \exp\left[p_{\text{bo5}}\left(\frac{r_{ij}}{r_0^{\pi\pi}}\right)^{p_{\text{bo5}}}\right] \end{aligned} \quad (2)$$

where  $\text{BO}_{ij}$  corresponds to the bond order between atoms  $i$  and  $j$ ,  $r_{ij}$  is the interatomic distance between those atoms,  $r_0$  terms represent equilibrium bond lengths for each bond type ( $\sigma$ ,  $\pi$ , double  $\pi$ ), and  $p_{\text{bo}}$ 's are empirical fitting parameters. Because eq 2 is continuous, it allows for smooth transitions between  $\sigma$ ,  $\pi$ , and double  $\pi$  bond character while yielding a differentiable potential energy surface (PES) that allows for the computation of interatomic forces. When uncorrected, however, this equation often overestimates bond orders between nonbonded neighbors and produces unphysical coordination numbers. To address these issues, a local overcoordination correction is performed on all 1–3 nearest neighbor pairs and over- and undercoordination terms ( $E_{\text{over}}$  and  $E_{\text{under}}$ ) are included in the total energy equation (eq 1). Over- or undercoordination is determined by comparing the bond order to the valency of the atoms involved in the bond. If the corrected bond order exceeds the valency of the atom, an energetic penalty for overcoordination is incurred. If the valency is larger, the system is stabilized by the  $E_{\text{under}}$  term.

The ReaxFF workflow begins with the user-defined atomic positions and atom type designations (i.e., C, H, O). From these atomic positions,  $E_{\text{vdW}}$  is calculated between all atom pairs. The Morse potential utilized for calculation of this term is shielded to prevent excessive repulsions between bonded atoms or next-nearest neighbors. Using the EEM,<sup>3</sup> the partial charge for each atom is then computed based on atomic positions, electronegativity, and hardness (and described more fulsomely in the next section). Once partial charges have been determined,  $E_{\text{Coul}}$  can be calculated using a shielded Coulomb potential computed between all atom pairs. The remaining partial energy contributions are bond-order-dependent. Bond orders are computed for each atom using eq 2 and are then corrected for local overcoordination. The corrected bond orders are used to determine  $E_{\text{bond}}$ ,  $E_{\text{over}}$ ,  $E_{\text{under}}$ , and  $E_{\text{lp}}$ . From these corrected bond orders, the valence and torsion angles are enumerated, and their respective energetic contributions ( $E_{\text{val}}$  and  $E_{\text{tors}}$ ) are calculated. Finally, these partial energy contributions are summed (along with any system-specific terms included in  $E_{\text{specific}}$ ) and the total ReaxFF energy and forces are complete for the current time step iteration.<sup>11,41</sup>

In regards to transferability, when using a ReaxFF force field, careful consideration of how the force field was trained is needed to assess its viability for the user's application. No ReaxFF parametrization, which typically utilizes QM data at the density functional theory (DFT) level, should be used as a "black box" for their application just because it incorporates interactions involving atomic elements of interest. To illustrate, the standard local-density (LDA)/generalized gradient (GGA) density functional approximations are typically not sufficient to calculate

the heat of formation of a metal oxide.<sup>23,29</sup> This is strikingly apparent in nickel oxide where the GGA will predict that  $\text{Ni}_2\text{O}_3$  (the  $\text{Ni}^{3+}$  oxidation state of nickel) is more stable than  $\text{NiO}$  (the  $\text{Ni}^{2+}$  oxidation state of nickel), which is not observed experimentally. Furthermore, the LDA/GGA approximation underpredicts both the band gap and magnetic moment of  $\text{NiO}$ . In this example, a ReaxFF parametrization that is not fit to additional data such as surface energy or heat of formation would not be a good candidate for an application relying on stable crystal structures. In addition, one should be careful when utilizing single reference quantum mechanical methods such as DFT and MP2 for training bond dissociation, as they might provide insufficient accuracy. In such scenarios multireference ab initio methods should be utilized as demonstrated by Müller and Hartke for disulfide mechanochemistry.<sup>38</sup>

In summary, careful examination needs to be taken of how the ReaxFF force field was parametrized before using it in an application of choice. A good resource for such examination is the publication that describes the development and intended applications of the force field and using good chemical judgment. Later we address some recent efforts to improve transferability to overcome these limitations.

## ■ MODELS OF CHARGE DISTRIBUTIONS IN REACTIVE FORCE FIELDS

**Electronegativity Equalization Method.** The EEM builds on the early works of Gasteiger and Marsili, who formulated an iterative method for evaluating partial charges in molecules based on the principles of electronegativity equalization.<sup>1</sup> The EEM method developed by Mortier et al. is theoretically justified from DFT and adopts the Parr and Pearson's definitions of atomic electronegativity and hardness<sup>2–4</sup> QEeq (or CEM) is a variation of the EEM method developed by Rappé and Goddard<sup>7</sup> that provides a definition for the atomic electronegativity and hardness parameters and introduces electrostatic screening through Slater type charge densities. In the context of the ReaxFF model, the EEM formulation probably best fits the description of the method used as the parameters are obtained empirically, and it does not use Slater type charge densities. Throughout this paper, we refer to EEM as the general class of charge distribution algorithms that encompasses variants such as CEM and QEeq.

EEM is based on the second order expansion of the electrostatic energy with respect to atomic charge.

$$E(q_1, q_2, \dots, q_N) = \sum_{i=1}^N \left( E_i(0) + \chi_i^0 q_i + \frac{1}{2} \sum_{j=1}^N H_{ij} q_i q_j \right) \quad (3)$$

$$H_{ij} = J_{ii}^0 \delta_{ij} + J_{ij}(1 - \delta_{ij}) \quad (4)$$

where  $N$  is the total number of atoms in the system,  $E_i(0)$  is the charge reference point at  $q = 0$  for atom  $i$ ,  $\chi_i^0 = (\partial E_i / \partial q_i)$  is the electronegativity of atom  $i$ ,  $q_i$  and  $q_j$  are the partial charges of atoms  $i$  and  $j$ , respectively,  $J_{ii}^0 = \partial^2 E_i / \partial q_i^2$  is the atomic hardness of atom  $i$ , and  $J_{ij} = 1.0 / [r_{ij}^3 + (1/\gamma_{ij})^{3/2}]^{1/3}$  is a shielded Coulomb potential where  $\gamma_{ij}$  is an electrostatic shielding parameter. It essentially poses the charge distribution problem as an optimization problem where the objective is to minimize the electrostatic energy under the net system charge constraint.

To solve for the partial charges in the stated optimization problem, we use the derivative of eq 3 with respect to atomic charge:

$$\chi_i(q_1, q_2, \dots, q_N) = \frac{\partial E}{\partial q_i} = \chi_i^0 + J_{ii}^0 q_i + \sum_{j \neq i}^N (J_{ij} q_j) \quad (5)$$

and solve it under the constraint of charge conservation

$$\sum_{i=1}^N q_i = 0 \quad (6)$$

A Lagrange multiplier  $\mu$  is utilized to minimize eq 3 under the constraint of charge neutrality, yielding

$$\mu = \frac{\sum_{i=1}^N \sum_{j=1}^N H_{ij}^{-1} (-\chi_j^0)}{\sum_{i=1}^N \sum_{j=1}^N H_{ij}^{-1} (1_j)} = \frac{\sum_{i=1}^N q_i^s}{\sum_{i=1}^N q_i^t} \quad (7)$$

where  $q_i^s$  and  $q_i^t$  are the pseudocharges for atom  $i$ . Consequently, two sets of linear equation are solved independently:

$$\begin{aligned} \sum_{i=1}^N \sum_{j=1}^N H_{ij}(q_i^s) &= \sum_{i=1}^N -\chi_i^0 \\ \sum_{i=1}^N \sum_{j=1}^N H_{ij}(q_i^t) &= \sum_{i=1}^N 1_i \end{aligned} \quad (8)$$

Finally, the charge of atom  $i$  is determined through the relation

$$q_i = q_i^s + \mu q_i^t \quad (9)$$

The EEM method has been used for close to 3 decades within reactive force fields but has significant shortcomings such as unphysical long-range charge transfer, nonlinear size dependent polarizability, and noninteger molecular charge. Therefore, we review three recent theoretical improvements that are starting to displace the EEM method in ReaxFF.

**New Alternatives to EEM.** Since EEM's development in the mid 1980s, there have been several attempts to remedy EEM's deficiencies with regards to its unphysical long-range charge transfer and metallic polarizability. Some of the most notable methods are the atom–atom charge transfer method (AACT),<sup>9</sup> split charge equilibration (SQE),<sup>17</sup> and charge transfer with current polarization equalization (QTPIE).<sup>16</sup> However, unlike the original EEM method, these earlier solutions are based on physical intuition as apposed to being derived from quantum chemistry.

The atom-condensed Kohn–Sham DFT to second order (ACKS2)<sup>25</sup> stands out from these previous efforts as it provides an extension of the original EEM method within an atom-in-molecule derivation from Kohn–Sham DFT. Verstraelen and co-workers revealed that EEM was missing nonlocal contributions of the kinetic energy, which were essential for eliminating the unphysical long-range charge transfer. In their derivation, the second order expansion of the kinetic energy introduces the Kohn–Sham linear response matrix ( $X_{ij}$ ), which can be interpreted as a measure of electron delocalization. Unfortunately, the exact relation between the Kohn–Sham linear response matrix and atomic coordinates is not trivial and simplified approximations are required. For practical purposes, the Kohn–Sham linear response matrix between two fragments is defined to exponentially decay to zero at large interatomic separations impeding long-range charge transfer.

$$E_{\text{ACKS2}} = \underset{\vec{q}}{\operatorname{argmin}} \left[ \sum_{i=1}^N \chi_i^0 q_i + \frac{1}{2} \sum_{i=1}^N \sum_{j=1}^N H_{ij} q_i q_j \right. \\ \left. + \underset{\vec{\mu}}{\operatorname{argmax}} \left[ \sum_{i=1}^N \mu_i (q_i - q_i^0) \right. \right. \\ \left. \left. + \frac{1}{2} \sum_{i=1}^N \sum_{j=1}^N X_{ij} \mu_i \mu_j \right] \right] \quad (10)$$

where  $\mu_i$  is the atomic Kohn–Sham potential of atom  $i$  and  $X_{ij}$  is a distance-dependent linear response matrix element that determines to what extent atoms  $i$  and  $j$  transfer charge. In Figure 1, it is shown that ACKS2 predicts that the charge and

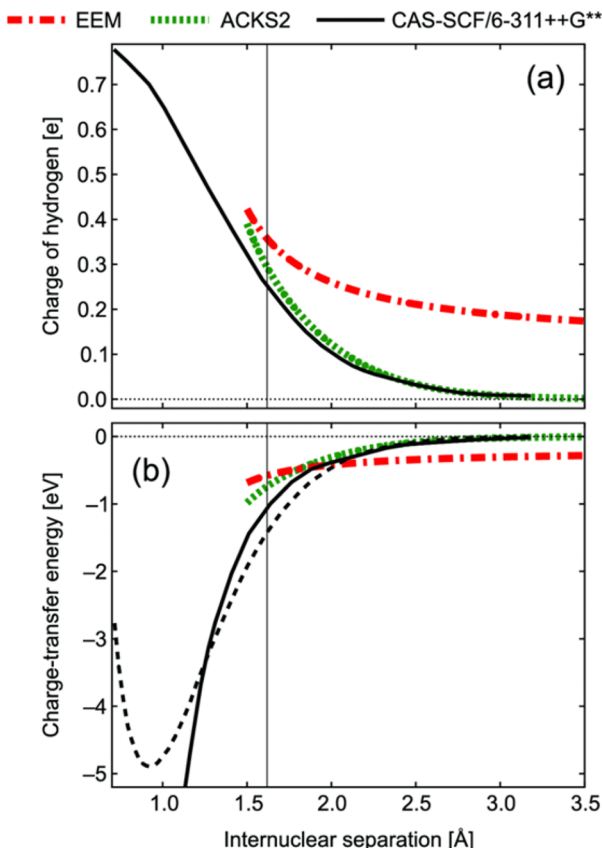


**Figure 1.** ACKS2 performance for hydrogen fluoride dissociation: (a) Charge of hydrogen as a function of hydrogen–fluoride distance. (b) Charge transfer energy as a function of a hydrogen–fluoride distance. Comparing EEM (red), ACKS2 (green), and CAS-SCF/6-311++G\*\*. Reprinted from ref 25, with the permission of AIP Publishing.

charge transfer energy in hydrogen fluoride approach zero at the limit of large separation. In regards computational expense, the ACKS2 model requires solving a  $(2N + 2) \times (2N + 2)$  matrix, and comparisons between the computational performance of EEM and that of ACKS2 are presented below. The ACKS2 model has recently been added to LAMMPS and is also available in the Purdue molecular dynamics software (PuReMD)<sup>28</sup> and in the Amsterdam Density Functional program (ADF).

**Toward More Explicit Representations of Electrons.** The ReaxFF/EEM approach models electrons implicitly in the bonded interactions, which has proven insufficient for several

applications.<sup>35</sup> For example, redox reactions modeled with standard ReaxFF impose charge constraints that are problematic for describing charge transfer in reactive environments.<sup>36</sup> ReaxFF also is not able to reproduce electron affinities (EAs) and ionization potentials (IPs) for most chemical species. An accurate description of these electron transport phenomena requires explicit treatment of electronic degrees of freedom.

**The eReaxFF Model.** eReaxFF expands upon the standard ReaxFF formalism by incorporating a pseudoclassical explicit electron/hole scheme.<sup>35</sup> The general expression for the eReaxFF total energy is

$$E_{\text{eReaxFF}} = E_{\text{ReaxFF}} + E_{\text{nuc-elec}} + E_{\text{elec}} \quad (11)$$

where partial energy contributions include all standard ReaxFF terms (see eq 1) with additional energy terms to account for electron–nucleus interactions ( $E_{\text{nuc-elec}}$ ) and electron–electron interactions ( $E_{\text{elec}}$ ). All many-body bonded and nonbonded interaction terms in ReaxFF are retained with modifications made to the functional forms of  $E_{\text{over}}$ ,  $E_{\text{under}}$ , and  $E_{\text{lp}}$  to incorporate the explicit electrons and holes. Note that while eReaxFF can mathematically describe holes as well as electrons, so far only eReaxFF descriptions using explicit electrons have been reported; as such we will limit the further discussion to electrons.

In eReaxFF, nuclei are treated as point charges and electrons as Gaussian wave functions of the form  $\psi \propto \exp(-\alpha(r - r')^2)$ . These Gaussian wave functions interact with the nuclei through the following pairwise interaction:

$$E_{\text{nuc}(i)-\text{elec}(j)} = -1/(4\pi\epsilon_0)\beta \sum_{i,j} \frac{Z_i}{R_{ij}} \operatorname{erf}(\sqrt{2\alpha} R_{ij}) \quad (12)$$

where  $Z$  is the nuclear charge,  $R_{ij}$  is the distance between the electron and nucleus, and  $\alpha$  and  $\beta$  are constants that depend on the atom type. The electron is represented as an additional particle bearing a  $-1$  charge; electron particles interact with all other atomic charges using the same shielded Coulomb interaction as in standard ReaxFF. The number of electrons associated with any single atom is determined by

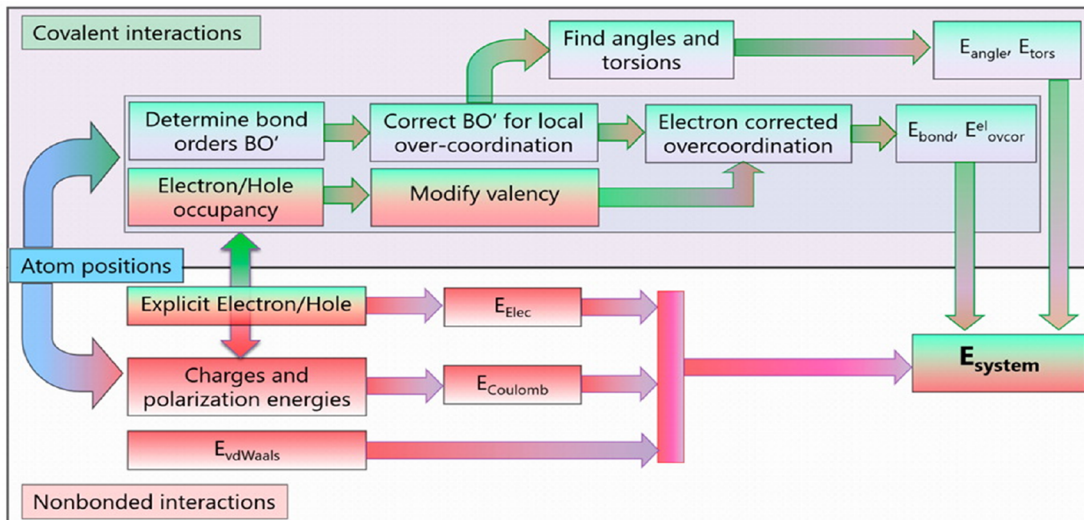
$$n_{\text{el}} = \exp(-p_{\text{val}} \cdot R_{ij}^2) \quad (13)$$

where  $R_{ij}$  is the distance between the atom-center and the electron and  $p_{\text{val}}$  is a Gaussian exponent. This enables the electron particle to hop between atoms, thus allowing electron transfer processes to be modeled by eReaxFF.

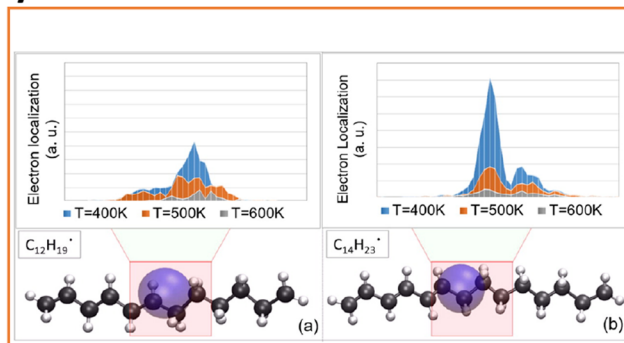
One of the biggest drawbacks of the standard ReaxFF formalism is that the bonded and nonbonded interactions are calculated independently. That is, the valency and number of lone-pair (valence) electrons for each atom type are independent of the partial atomic charges. This decoupling of the bond order and atomic charges can give rise to unphysical behavior of ions. For example, based on its atom type, standard ReaxFF would assign a hydrogen cation ( $H^+$ ) a valency of one, despite its positive charge. By introducing variable valency and coupling the number of lone-pair electrons of an atom to the proximity of explicit electrons, eReaxFF is capable of modeling charge transfer in reactive systems more accurately than ReaxFF. As shown in the flowchart in Figure 2a, the eReaxFF method retains the basic framework of ReaxFF.

As in the original ReaxFF, the user provides atomic positions and atom type designations (i.e., C, H, O). Additionally, the user defines explicit electrons as atoms with their own sets of Cartesian coordinates. In all current implementations, electrons

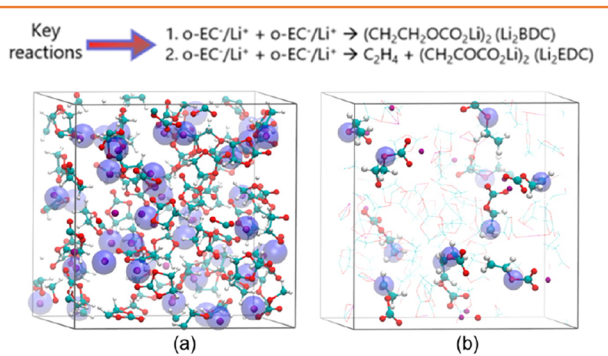
(a)



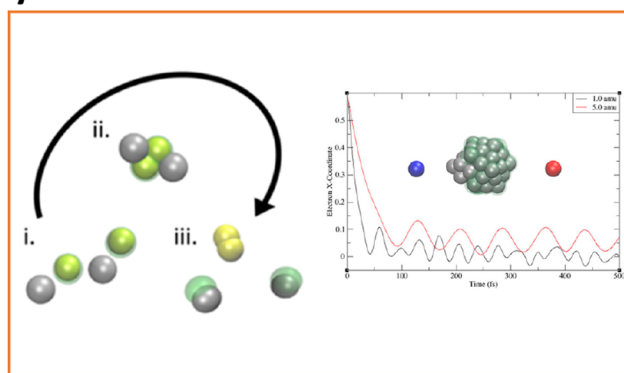
(b)



(c)



(d)



(e)

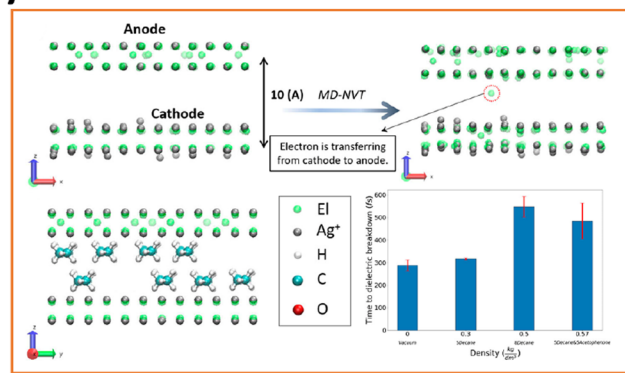


**Figure 2.** Applications of the eReaxFF: (a) eReaxFF workflow.<sup>35</sup> (b) Time-averaged electron localization near the contact point of aliphatic and conjugated chains of  $C_{12}H_{19}$  (left) and  $C_{14}H_{23}$  (right) at different temperatures.<sup>35</sup> Panels a and b reproduced from ref 35. Copyright 2016 American Chemical Society. (c) Snapshot of eReaxFF MD at  $t = 0$  ps (left) and  $t = 25$  ps (right) with produced  $o\text{-EC}/\text{Li}^+$  radicals highlighted; Li ions and EC molecules not involved in the electron-transfer events are shown as lines. Reproduced from ref 36. Copyright 2016 American Chemical Society. (d) Reduction mechanism of  $2\text{AgCl}$  at elevated temperatures (left), where two sets of  $\text{AgCl}$  pairs align with one another (i) before  $\text{Cl}$  (yellow spheres) aggregates to form  $\text{Cl}_2$  (ii), while excess electrons (green spheres) are transferred from  $\text{Cl}_2$  to  $\text{Ag}^+$  ions (silver spheres), yielding  $2\text{Ag}^0$  atoms (iii); plasmonic oscillations (right) of initially polarized  $\text{Ag}_{55}$  between positive (red sphere) and negative (blue sphere) charges at  $T = 300$  K. Reproduced from ref 57. (e) TDDB of PE (top), where TDDB is taken as the time of first electron transfer from anode to cathode, addition of 5 decane and 5 acetophenone molecules into vacuum between electrodes (bottom left), and effect of increased PE density and presence of acetophenone on TDDB (bottom right). Reproduced from ref 66.

are assigned a mass of 1 amu in order to facilitate femtosecond-range simulation time steps. Interactions between electrons and atomic nuclei ( $E_{\text{nucl-elec}}$ ) are calculated using eq 12. Partial charges in eReaxFF are computed using the ACKS2 method

rather than the EEM method employed by standard ReaxFF (see [Models of Charge Distributions in Reactive Force Fields](#)). Using a shielded Coulomb potential, the electrostatic energy contribution ( $E_{\text{Coul}}$ ) is computed from the ACKS2 partial

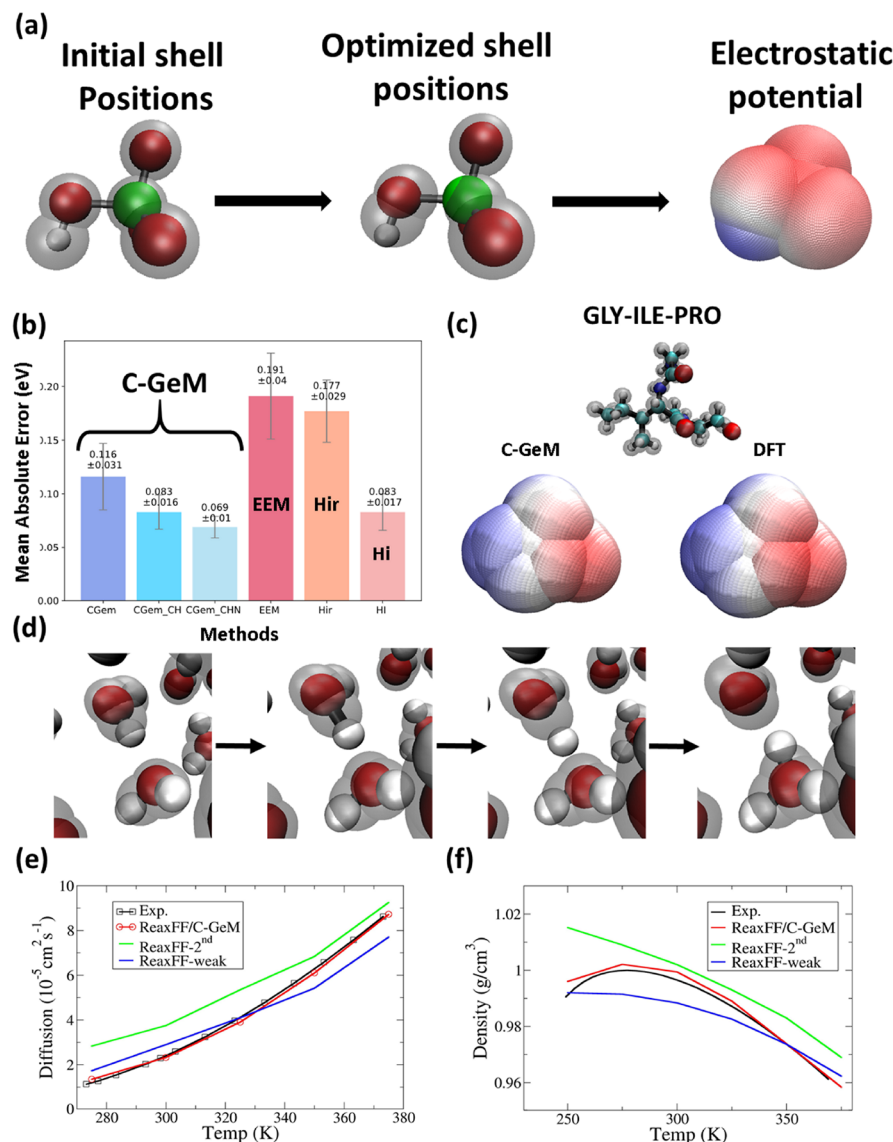


**Figure 3.** C-GeM model: (a) Schematic showing the basic principle of the C-GeM model starting with an initial guess for the electronic shell positions that are optimized within the nuclear core field, which are then used to generate the ESP of the molecule. (b) MAE with respect to the DFT ESP ( $\omega b97X-V/\text{def2-qzvpp}$ ), comparing C-GeM (purple), C-GeM with atom types C and H (light blue), C-GeM with atom types C, H, and N (light green), EEM (red), Hirschfeld charges (orange), and iterative Hirshfeld (pink). (c) ESP of the tripeptide Gly-Ile-Pro showing the C-GeM (left) and DFT (right) ESP. (d) Frame from a constrained dynamics simulation showing autodissociation of water to hydronium and hydroxide using the ReaxFF/C-GeM model. (e) Diffusion and (f) density of water as a function of temperature comparing the ReaxFF/C-GeM (red) with ReaxFF-second (green), ReaxFF-weak (blue), and experiment (black). Adapted with permission from refs 53 and 60. Copyright 2019 and 2020 American Chemical Society.

charges. All nonbonded interactions have now been accounted for, leaving only bond-order-dependent terms. The bond orders are calculated in the same manner as described for the original ReaxFF.

The fundamental difference between standard ReaxFF and eReaxFF is the modification of atom valency based on its proximity to an explicit electron. First, the electron occupancy is determined using eq 13, and the valency of any affected atoms are modified accordingly. For example, consider a neutral oxygen atom with its six valence electrons and valency of two. Should that oxygen atom gain a seventh valence electron, it may only form one bond, and its valency is reduced to one. This decreased valency results in a larger overcoordination penalty and reduces the bond order associated with the atom. These electron-corrected bond orders are used to compute the

energetic contributions from the chemical bonds ( $E_{\text{bond}}$ ), the overcoordination penalty ( $E_{\text{over}}$ ), and the lone pair electrons ( $E_{\text{lp}}$ ). In contrast to ReaxFF, this scheme has enabled the eReaxFF method to counteract the formation of unphysical bonds such as  $\text{H}^+ - \text{H}^+$  due to the higher overcoordination penalty stemming from the loss of valence electron from the H atom. Finally, the partial energy contributions are summed (along with any system-specific terms in  $E_{\text{specific}}$ ), and the total eReaxFF energy is reported for the iteration.

The eReaxFF method has been successfully employed to study electron transfer in hydrocarbons,<sup>35</sup> solid–electrolyte interfaces,<sup>36</sup> Ag-metal systems,<sup>57</sup> and recently electrical breakdown in polyethylene (PE).<sup>66</sup> Islam et al. performed eReaxFF MD simulations on two representative hydrocarbon radicals,  $\text{C}_{12}\text{H}_{19}$  and  $\text{C}_{14}\text{H}_{23}$ , at different temperatures, finding that longer

aliphatic chain length slows down electron transfer (Figure 2b).<sup>35</sup> Additionally, they found that an increase in temperature accelerates electron transfer but decreases electron localization around the junction. eReaxFF was also employed to study the major reduction reaction pathways of ethylene carbonate (EC) in Li-ion batteries.<sup>36</sup> In this study, eReaxFF properly captured the electron transfer event from Li to EC (forming EC<sup>-</sup>/Li<sup>+</sup>), the subsequent C–O bond cleavage (forming o-EC<sup>-</sup>/Li<sup>+</sup> radical), and radical termination reactions (forming dilithium butyl/ethyl dicarbonate) (Figure 2c).<sup>36</sup> eReaxFF has also been extended to reproduce isomerization energies, electron affinities (EAs), and ionization energies (IEs) of small neutral and charged Ag nanoclusters.<sup>37</sup> This Ag-metal force field introduces a quasi-Drude atomistic description into eReaxFF with every neutral atom being represented by a paired cation and electron (i.e., a neutral Ag atom becomes a Ag<sup>+</sup> cation and an explicit electron). With this additional electronic degree of freedom, it becomes possible to model the reduction of Ag<sup>+</sup> to Ag<sup>0</sup> by Cl<sub>2</sub> and the resulting aggregation and growth of the nascent Ag cluster. One novel functionality introduced by the quasi-Drude model is the ability to model plasmonic motion by tracking the movements of the explicit electrons throughout a simulation (Figure 2d).<sup>37</sup> In another recent study, eReaxFF was used to simulate the electrical breakdown of polyethylene (PE), exploring the roles of byproducts and processing parameters such as density on the time to dielectric breakdown (TDDB) of PE (Figure 2e).<sup>66</sup> These simulations indicate that increased PE density enhances the TDDB, while adding species with positive EA (i.e., acetophenone byproducts) reduces the TDDB. The eReaxFF method is currently available in van Duin's standalone ReaxFF code and in the ADF program.

**The C-GeM Model.** C-GeM is an alternative explicit electron density method recently proposed by Leven and Head-Gordon for treating electrostatics in molecular simulations.<sup>53</sup> In C-GeM, atoms are represented by a positively charged core and a negatively charged shell treated as Gaussian charges. C-GeM uses the Born–Oppenheimer approximation in which electronic shells are treated as massless particles that are instantaneously optimized within the field generated by the nuclear cores. The interactions between the cores and shells comprise an electrostatic term:

$$E_{ij}^{\text{elec}}(r_{ij}) = \frac{(q_i \cdot q_j)}{r_{ij}} \operatorname{erf}\left(\sqrt{\frac{(\alpha_i \cdot \alpha_j)}{(\alpha_i + \alpha_j)}} r_{ij}\right) \quad (14)$$

$$\alpha_i = \frac{\gamma}{(2R_i)^2}$$

where  $r_{ij}$  is the distance between core  $i$  and shell  $j$ ,  $q_i$  and  $q_j$  are the core and shell charges,  $R_i$  and  $R_j$  are the core and shell radii, and  $\gamma$  is a global parameter. In addition C-GeM comprises a Gaussian term which is given by

$$E_{ij}^{\text{Gauss}}(r_{ij}) = A_i e^{(-\gamma r_{ij}^2)} \quad (15)$$

$$\gamma_i = \frac{\omega}{(2R_i)}$$

where  $A_i$  is the magnitude of the Gaussian interaction determined by the electronegativity of core  $i$  and  $\omega$  is a global parameter. In C-GeM, the sum of the electrostatic and Gaussian terms at complete overlap is defined as the electronegativity of a given atom type as shown in the following expression:

$$\chi_i = E_{ij}^{\text{Gauss}}(r_{ij} = 0) + E_{ij}^{\text{elec}}(r_{ij} = 0) \quad (16)$$

where  $\chi_i$  is the electronegativity of atom  $i$  and  $E_{ij}^{\text{Gauss}}(r_{ij} = 0)$  and  $E_{ij}^{\text{elec}}(r_{ij} = 0)$  are the Gaussian and electrostatics components, respectively, at a core–shell distance of  $r_{ij} = 0$ . The total energy of the system is then given by the sum over all cores and shells:

$$E_{\text{C-GeM}} = \sum_i^n \sum_{j < i}^n (E_{ij}^{\text{elec}}(r_{ij}) + E_{ij}^{\text{Gauss}}(r_{ij})) \quad (17)$$

Here  $E_{\text{C-GeM}}$  is the total C-GeM energy,  $n$  is the number of cores + shells in the system and  $r_{ij}$  is the distance between particles  $i$  and  $j$ . Accordingly, in the SCF regime, the positions of the shells are found by minimizing the following equation:

$$\frac{\delta E_{\text{C-GeM}}}{\delta r_{\text{shell}}} = 0 \quad (18)$$

C-GeM was first developed to reproduce the electrostatic potential (ESP) of molecules containing pure C, H, O, and Cl elements as demonstrated in Figure 3a. The C-GeM model shows good accuracy with an average absolute mean deviation from the reference DFT ESP ( $\omega b97X-V/\text{def2-qzvpp}$ )<sup>30</sup> of 0.11 eV compared to 0.21 eV for the EEM and competitive with the 0.06 eV of ab initio generated charges such as those obtained by iterative Hirschfeld partial charges.

As a purely electrostatic model, C-GeM has been adapted with parameters specifically fitted for protein electrostatics, that is, by atom-typing of C, H, N, and O according to their versatile bonding in organic chemistry. This improves the mean absolute error (MAE) to the ab initio ESP to 0.071 eV for C-GeM, now outperforming iterative Hirshfeld at 0.083 eV and EEM at 0.191 eV, Figure 3b,c. For this set of tripeptides fragmented from protein structures (with an average size of 46 atoms), Protein C-GeM predicts the ESP at a speed of 0.9 s per structure vs the EEM solution, which takes 0.2 s, which is very competitive given its much greater accuracy. In fact, it outperforms iterative Hirschfeld at costs that are 4–5 orders of magnitude cheaper in computational expense. Thus, the accurate and fast protein C-GeM is potent for many applications such as fast protein electrostatic screening or serving as part of scoring function in docking in drug discovery.

One of the significant drawbacks of the EEM method is its inability to dissociate molecules to integer charged fragments and unphysical long-range charge transfer. Leven and Head-Gordon<sup>53</sup> demonstrated that C-GeM can account for the dissociation of hydrogen chloride to the ionic products Cl<sup>-</sup> and H<sub>3</sub>O<sup>+</sup> in solution, in good agreement using ab initio MD trajectories of HCl dissociation in water. Recently, Leven et al.<sup>60</sup> have developed a reactive water model by integrating C-GeM within the framework of the ReaxFF. One of the advantages in using C-GeM is its ability to correctly assign charges in scenarios involving ionic molecules. Figure 3d shows constrained dynamics trajectories of water autodissociation using the ReaxFF/C-GeM model presenting the dissociation of water to hydronium and hydroxide ions. In addition, bulk water properties were compared to two recent ReaxFF water force fields, showing superior performance of the ReaxFF/C-GeM model. Figure 3e plots the diffusion as a function of temperature showing great agreement between the ReaxFF/C-GeM model and experiments. Figure 3f plots the density as a function of temperature showing that the ReaxFF/C-GeM model can reproduce the maximum density of water.

**Electrostatic Embedding Using ReaxFF/C-GeM.** The Head-Gordon group<sup>65</sup> has recently advanced a ReaxFF/C-GeM model by performing electrostatic embedding using nonreactive force fields, similar to that of QM/MM methodologies. Such an approach will benefit the high efficiency and reasonable accuracy of nonreactive force fields at long range while still being able to account for chemical reactivity in a local region of the system. Similar to QM/MM methods, atoms are split into three categories: (i) ReaxFF/C-GeM atoms, which include all atoms in the chemically reactive region, (ii) the MM atoms, which include all remaining atoms and is handled exclusively by the nonreactive force field, and (iii) the van der Waals and electrostatic nonbonded interactions between the ReaxFF/C-GeM region and the MM region.

The ReaxFF/C-GeM hybrid model has recently been applied to the study of proton hopping in confined acidic nanometer-sized reverse micelles,<sup>65</sup> which is an important model system to help our understanding of charge transport in a wide range of chemical and biological processes,<sup>43</sup> especially for environments under confinement and at interfaces.<sup>20,44</sup> The reverse micelle spontaneously forms by self-assembly in which the amphiphilic nature of surfactants in a nonpolar solvent causes them to organize to encapsulate a water pool as depicted in Figure 4. The

concentrations of HCl were simulated by replacing waters with ions to reproduce experimental acid concentrations.

From the ReaxFF/C-GeM reactive molecular dynamics simulations, which were able to reproduce the terahertz and dielectric relaxation data on the exact same systems, we found a surprising change in the proton hopping mechanism as hydronium ion concentration increases. More specifically, we found a switch in the dominant Grotthuss proton hopping mechanism for small reverse micelles to one in which localized oscillatory hopping emerges as the dominant mechanism at a critical micelle size also seen experimentally. This change stems from the accumulation of hydronium and chloride ions at the micelle interface, which creates a short-circuited hydrogen-bonding network for proton hops; that is, as the micelle size or acid concentration increases, the interfacial water network induces a “traffic jam” that favors the localized oscillatory hopping mechanism.

## ■ SOFTWARE ADVANCES FOR REACTIVE FORCE FIELDS

The code for the ReaxFF method was originally implemented by van Duin as a sequential Fortran based program that still serves as the reference implementation in regards to accuracy of energy and force calculation. ReaxFF is also available in the PuReMD software<sup>28</sup> in both distributed memory parallel and multi-GPU parallel versions.<sup>21,37</sup> In addition to its standalone version, PuReMD has been integrated into the open-source large-scale atomic/molecular massively parallel simulator (LAMMPS) as the USER-ReaxC package. Later, a hybrid OpenMP/message passing interface (MPI) parallel version of this package optimized for multicore architectures<sup>50</sup> was released in the LAMMPS USER-OMP package. The ReaxFF method is also available in other important simulation environments, including the ADF program and Materials Studio released under license by Biovia (<https://www.3dsbiovia.com>), as well as Nanohub (<http://www.nanohub.org>).

**ReaxFF Parallel Implementation in LAMMPS.** LAMMPS uses the highly scalable domain-decomposition method, along with MPI, for large distributed-memory parallel computations.<sup>8</sup> The ReaxFF capability in LAMMPS (USER-ReaxC) is originally based on PuReMD, as is the QE<sub>q</sub> charge equilibration method in LAMMPS. Traditionally, the QE<sub>q</sub> charge equilibration method has been used with ReaxFF. However, QE<sub>q</sub> has been shown to be problematic for isolated atoms or molecules, where the ACKS2 method should be used instead.<sup>25</sup> A fully MPI-enabled ACKS2 method has been implemented in LAMMPS, based on a serial PuReMD implementation.<sup>62</sup> LAMMPS uses the Kokkos library<sup>26</sup> on top of MPI, for performance portability. Kokkos abstractions allow a single c++ kernel to run on different hardware, that is, GPUs and multicore CPUs.

In order to investigate the performance of ReaxFF in LAMMPS, a water system was run on Intel Skylake (Xeon 6140) CPU as well as NVIDIA V100-16GB GPU (connected to IBM Power9 CPU) hardware. Both the QE<sub>q</sub> and ACKS2 charge equilibration methods were used. We note that when running on the GPU using the Kokkos version of ReaxFF, it is important to use the “full” neighbor-list option for QE<sub>q</sub> for performance, which eliminates the need for thread-level atomics, at the cost of redundant computation in the sparse-matvec. Figure 5a shows performance vs system size on a single CPU node or single GPU per node. CPU performance is relatively flat versus system size, while GPU performance is better for larger systems. Figure 5b

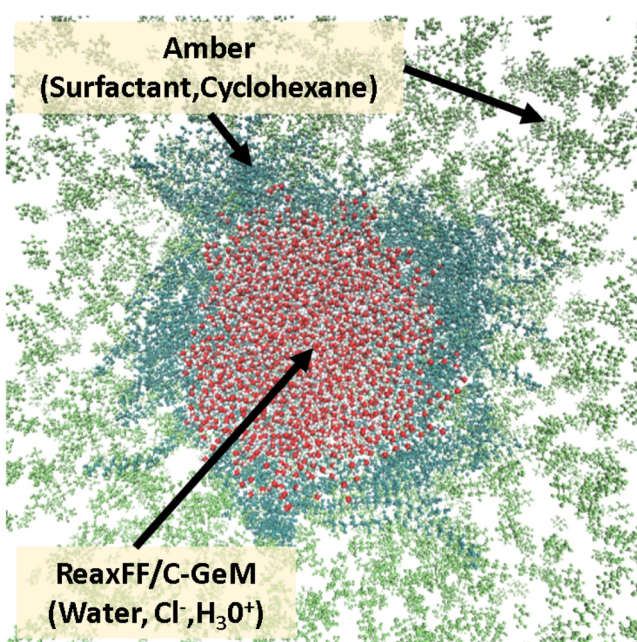


**Figure 4.** Schematic presentation of modeling a reverse micelle using a hybrid ReaxFF/C-GeM+Amber hybrid model: Snapshot of the reverse micelle with diameter = 5.96 nm; the water pool is treated with the Reaxff/C-GeM model (oxygen, red; hydrogen, white); surfactants (dark green) and cyclohexane solvent (light green) were treated with the amber force field.

water pool is encapsulated by the Igepal CO-520 surfactants (shown in dark green) with the hydrophilic headgroup, and the hydrophobic group is directed to the cyclohexane solvent (light green). The reverse micelles were first equilibrated with classical MD simulation using the general Amber force field (GAFF)<sup>15</sup> to account for the cyclohexane and surfactant molecules with AM1-BCC<sup>10</sup> charges obtained by ANTECHAMBER,<sup>12</sup> and the TIP3P water was used for the equilibration of the water pool. Then the water pool was replaced with the ReaxFF/C-GeM water model and further equilibrated. Then various concen-

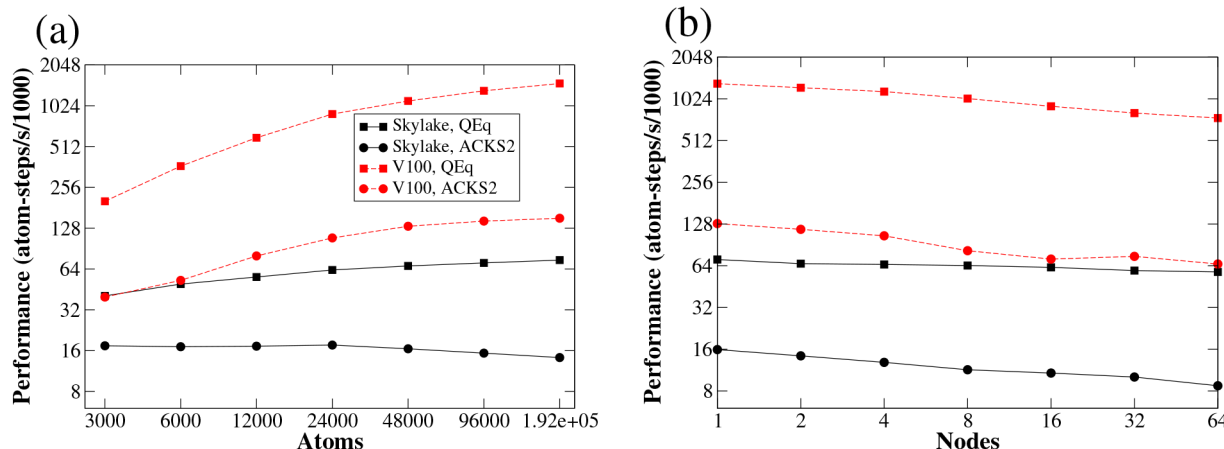


**Figure 5.** LAMMPS overall performance (thousand atom time steps per second) for a ReaxFF water system versus (a) system size, running on a single CPU node or GPU, and (b) node count, weak scaling 96000 atoms per node. Black curves represent Intel Skylake CPU hardware, and red curves represent NVIDIA V100 GPU hardware. Squares represent the QEq method, while circles represent the ACKS2 method. Higher is better, and ideal scaling is a horizontal line.

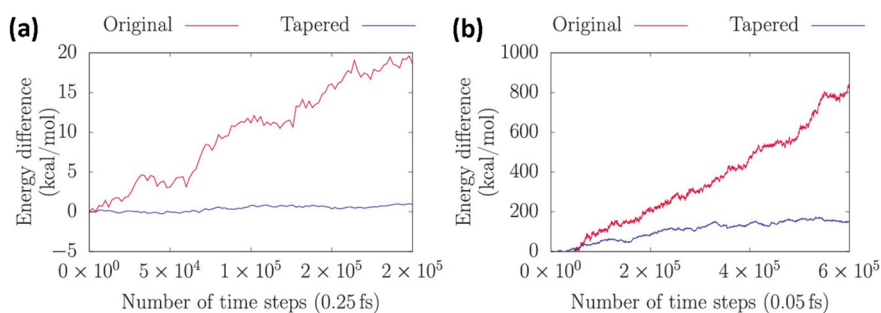


**Figure 6.** Total energy conservation during NVE dynamics for original (red line) and tapered (blue line) ReaxFF: (a) Trpzip2 peptide; (b) TNT single crystal. Reprinted with permission from ref 52. Copyright 2019 American Chemical Society.

shows performance vs node count when weak scaling 96000 atoms per node.

**Energy Conservation in ReaxFF.** A known flaw of the traditional ReaxFF formulation is its lack of appropriate energy conservation in the NVE ensemble. While thermostats are usually applied in applications of MD, which can tolerate small energy drifts, lack of energy conservation implies a defective PES and imperfect forces acting on the atoms. A recent paper by Furman and Wales identified the origins of energy drifts due to discontinuities in the PES, which result from distance cutoffs used in the bonded interaction terms of ReaxFF.<sup>52</sup> In order to repair the flaws in the PES, they applied a 7th degree polynomial tapering function to the bond order and bonded energy terms. A high degree polynomial tapering function was utilized since it satisfies the requirement of smooth first and second order derivatives at the cutoff distances and low computational overhead.

Figure 6a,b compare the energy drift in the NVE ensemble with and without the tapered bond energy terms of the Trpzip2 peptide and TNT crystal systems, respectively. It is evident that the tapered PES successfully reduces the energy drifts by more than an order of magnitude with respect to the original ReaxFF PES. However, one should be cautious when applying the tapering function correction as the modification in the PES can alter systems properties and therefore a reparametrization of the force field might be necessary. For example, the density of the TNT crystal changed from 1.59 g/cm<sup>3</sup> in the original ReaxFF to 1.69 g/cm<sup>3</sup> in the tapered corrected PES. It is worth mentioning

a subsequent paper from the same group that proposed modifications of various ReaxFF energy terms with an aim to further improve the stability and accuracy of ReaxFF.<sup>58</sup>

**Hybrid Models in LAMMPS.** It is relatively straightforward to conduct a ReaxFF/MM simulation in the LAMMPS code. Along these lines, a hybrid ReaxFF/AMBER MD tool, which introduces bond breaking and formation capabilities within the AMBER MD software package, was recently introduced.<sup>63</sup> This tool enables the study of local reactive events in large systems at a fraction of the computational costs of QM/MM models. For this ReaxFF/AMBER MD integration, AMBER is the simulation driver. AMBER categorizes atoms into the core ReaxFF, transition (ReaxFF/MM), and AMBER atom groups; it sends all relevant information for core ReaxFF and ReaxFF/MM atoms to the ReaxFF program. The ReaxFF/AMBER tool currently uses the external model interface; that is, the necessary data transfers between ReaxFF and AMBER are performed using file-based data exchange (a full fledged software integration is in the works). After AMBER writes the data exchange files, it launches the ReaxFF program as an external binary. The ReaxFF program then runs a zero-step nonperiodic simulation to calculate the dynamic charges, energies, and forces on the ReaxFF and ReaxFF/MM atoms and writes this information back into another file for AMBER to read.

In implementing the interface between the ReaxFF and AMBER programs, the following procedure is currently adopted by the ReaxFF/AMBER software:

- Dynamic charges on ReaxFF atoms are calculated under the influence of ReaxFF/MM atoms with static charges using QEq.
- All interactions between ReaxFF–ReaxFF atom pairs are calculated without any modifications.
- Electrostatic interactions between ReaxFF (with dynamic charges) and ReaxFF/MM (with static charges) atom pairs are calculated by ReaxFF.
- van der Waals interactions between ReaxFF–ReaxFF/MM atom pairs are handled by AMBER (e.g., using a Lennard-Jones potential).
- Interactions between MM–ReaxFF/MM and MM–MM pairs are handled by AMBER as usual.

It should be noted that there are some limitations of the current ReaxFF/AMBER tool. Currently, only systems with noncovalent bonds between ReaxFF and ReaxFF/MM regions can be studied. Also, only shared memory parallelism can be leveraged for the ReaxFF region. Nevertheless, the current implementation serves as a proof-of-concept of the feasibility and advantages of the hybrid approach<sup>63</sup> and proved robust for our implementation of the ReaxFF/C-GeM/Amber model to consider proton hopping mechanisms in acidic nanopools of reverse micelles.<sup>65</sup>

## METHODS FOR ACCELERATING REACTIVE FORCE FIELDS

Preconditioners generally transform the set of linear equations for improving their spectral properties. A recent study compared the performance of several preconditioners on the convergence of EEM and demonstrated that a significant reduction in computational time can be achieved by applying incomplete factorization and sparse approximate inverse (SAI) preconditioners.<sup>61</sup> Another recent addition is the development of extended Lagrangian schemes that have been demonstrated to reduce the computational cost of EEM significantly. The inertial extended Lagrangian/self-consistent scheme method (iEL-SCF) reduces the number of SCF iterations by allowing sufficient energy conservation with a high convergence tolerance.<sup>54</sup> An additional extended Lagrangian method is the stochastic constrained extended Lagrangian molecular dynamics (SC-XLMD), which eliminates the requirement for SCF altogether by propagating the charges and chemical potential along with the atomic degrees of freedom and applying holonomic constraint to ensure charge conservation.<sup>54</sup> Here we review these new algorithms for improving reactive force field performance with focus on ReaxFF specifically.

**Preconditioned Solvers.** Solution of large sparse linear systems required for charge equilibration models constitutes a significant bottleneck against scalability of ReaxFF simulations. More precisely, the sparse linear solvers may start accounting for a significant portion of the execution time in large runs due to communication overheads. O’Hearn et al. have addressed this issue in a series of publications. First, they presented a number of incomplete LU (ILU) based preconditioning techniques and their parallelization on shared memory architectures.<sup>39</sup> They have shown that these techniques significantly accelerate the Krylov subspace solvers for the QEq, EEM, and ACKS2 charge models (from tens of iterations per step to as low as a few iterations).

However, ILU based preconditioners are inherently sequential, and therefore they do not lend themselves for scalable distributed memory parallelization. For this reason, they next

investigated sparse approximate inverse (SAI) preconditioning techniques, as those can easily be scaled to large systems.<sup>61</sup> SAI preconditioners are generally less effective than ILU techniques. However, they were able to identify sparsity patterns in SAI that allow QEq, EEM, and ACKS2 solvers to converge at about the same rate as ILU based techniques. In fact, their experiments on shared memory systems have shown that SAI solvers outperform ILU ones as a result of their better parallelizability properties.

Recently, they have developed efficient distributed memory parallel implementations of the SAI preconditioning based solvers mentioned above.<sup>55</sup> The basic conjugate gradient (CG) solver used in parallel ReaxFF implementations utilizes the simple Jacobi (diagonal) preconditioner and requires tens of iterations per step for convergence. The newly developed distributed memory parallel SAI implementation leverages problem-specific characteristics of ReaxFF for high efficiency and scalability. The resulting solver significantly outperforms the Jacobi preconditioning based solvers in terms of rate of convergence and execution time as demonstrated by numerical tests (see below). To ensure high scalability, the new solver implementation utilizes a communication-hiding conjugate gradient scheme, specifically the pipelined CG (PIPECG) algorithm that reduces the number of global communications to only one nonblocking global reduction per iteration that can actually be overlapped with the preconditioner application and sparse matrix vector multiplication (SpMV) operation at the expense of some increase in vector operation costs.<sup>27</sup>

For numerical tests, two molecular systems comprised of bulk water ( $\text{H}_2\text{O}$ ) and amorphous silica ( $\text{SiO}_2$ ) were selected. These performance experiments were performed on the Cori supercomputer at the National Energy Research Scientific Computing Center (NERSC). In Table 1, we present the mean solver

**Table 1. Mean Solver Iterations for the Jacobi and SAI Preconditioned QEq Solvers**

data set	tolerance	solver	iterations
silica	$10^{-6}$	CG + Jacobi	11.8
		PIPECG + SAI	1.9
	$10^{-10}$	CG + Jacobi	39.2
		PIPECG + SAI	5.8
	$10^{-6}$	CG + Jacobi	9.5
		PIPECG + SAI	2.7
water	$10^{-6}$	CG + Jacobi	38.4
	$10^{-10}$	PIPECG + SAI	10.2

iterations for the Jacobi and SAI preconditioned QEq solvers at  $10^{-6}$  and  $10^{-10}$  tolerances for the 864000 atom silica and 837000 atom water systems using 512 processes. SAI preconditioning significantly improves the convergence rate of QEq compared to Jacobi preconditioning, yielding about 3.5 and 6 times faster convergence rates at  $10^{-6}$  tolerance for silica and water, respectively. The margin between SAI and Jacobi preconditioning gets larger as we go to  $10^{-10}$  tolerance threshold both for silica and water systems. Other tests (not shown here) indicate that this trend continues as we move to even smaller tolerances, e.g.,  $10^{-14}$ .

In Figure 7, the strong scaling plots for mean QEq time of preconditioned solvers for the silica and water systems are shown. Panels from left to right within a row show results at convergence tolerance levels of  $10^{-6}$  and  $10^{-10}$ . There are four different solver variants, starting with the basic CG + Jacobi solver and progressively advancing to the PIPECG + SAI solver.

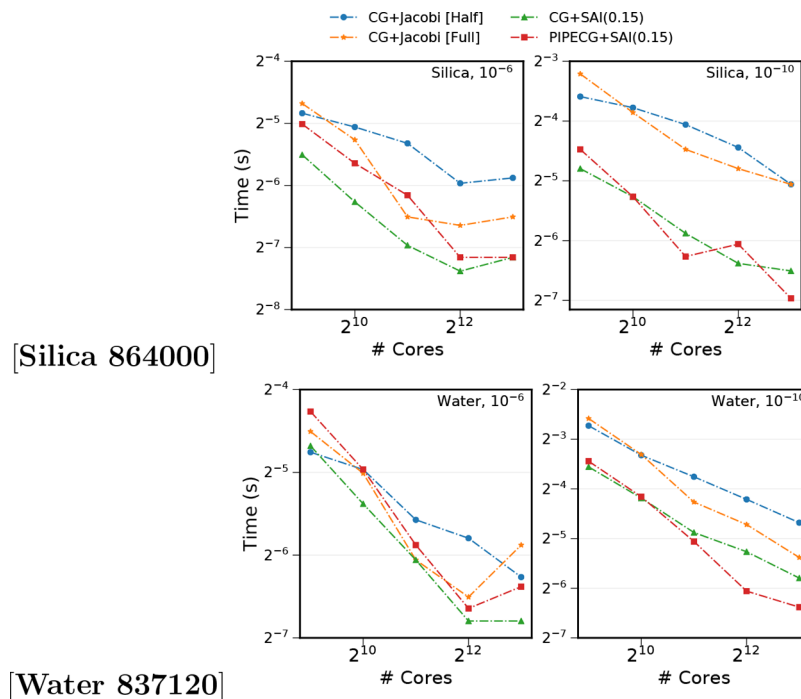


**Figure 7.** Strong scaling plots for mean  $Q_{eq}$  time of four preconditioned solvers for the silica and water systems. Figures from left to right within a row show results at convergence tolerance levels of  $10^{-6}$  and  $10^{-10}$ .

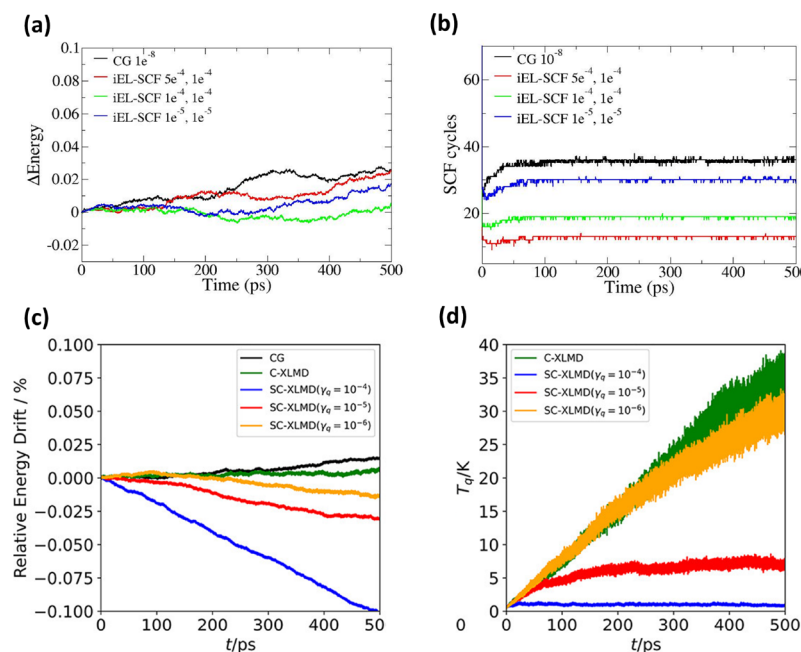


**Figure 8.** iEL-SCF and sc-XLMD extended Lagrangian methods for accelerating EEM. (a, b) Comparing the energy conservation and SCF cycles of CG-SCF at  $\epsilon^{-8}$  level of convergence with iEL-SCF using various levels of convergence tolerance of  $q_{SCF}^s$  (right) and  $q_{SCF}^t$  (left) for the  $FeOH_3$  system: (a) energy conservation; (b) SCF cycles. (c, d) Comparison of methods for energy conservation and latent charge temperature of the SC-XLMD simulation for bulk water. (c) Total relative energy drift in percentage units as a function of time for CG (10–10 convergence criteria), an extended Lagrangian with no latent variable thermostating (C-XLMD), and when using SC-XLMD with various values of the latent thermostat coupling parameter  $\gamma_q$ . The absolute value of energy drift rates in percent  $ns^{-1}$  are 0.03 (CG), 0.01 (C-XLMD), 0.22 (SC-XLMD with  $\gamma_q = 10^{-4}$ ), 0.05 ( $\gamma_q = 10^{-5}$ ), and 0.03 ( $\gamma_q = 10^{-6}$ ). (d) Corresponding latent charge temperature as a function of time for the above methods except CG. a-b reproduced from ref 54 with permission from the PCCP owner societies. c-d adapted with permission from ref 53 and 64 2020 American Chemical Society.

As expected, the fully optimized PIPECG + SAI version exhibits the best overall performance in large core counts. At  $1 \times 10^{-6}$  tolerances speed-ups up to  $2.4\times$ , and at  $10^{-10}$  tolerances speed-ups up to  $4.6\times$  are observed from PIPECG + SAI over the original QE solver in PuReMD.

The distributed memory parallelization work described above focused on the  $Q_{eq}$  model. While O’Hearn et al. have developed an effective generalized minimal residual (GMRES) based solver for ACKS2 in ref 61, unfortunately GMRES is not a nicely parallelizable solver, and CG does not work for ACKS2 due to

the indefinite nature of the matrices. However, it is possible to extend these preconditioning techniques to the ACKS2 model using a biconjugate gradient stabilized (BiCGStab) solver.

**Extended Lagrangian Methods for Solving Charge Equilibration.** EEM is an essential component of ReaxFF, allowing for charge rearrangement as bonds break and form; however, the self-consistent solution of two sets of linear equations at each time step is associated with a high computational cost. Therefore, numerous efforts are being made to decrease the computational cost of EEM, which will allow application of ReaxFF on larger scales. Recently, Leven and Head-Gordon applied the inertial extended Lagrangian self-consistent field method (iEL-SCF), originally developed for solving induced polarization, for solving EEM.<sup>53</sup> In the iEL-SCF method, auxiliary charges are introduced and propagated with respect to a harmonic potential around the real charges, which serve as an initial guess for the CG SCF solution of the real charges. As shown in eq 8, determining the partial charge in EEM requires solving two separate sets of linear equations. Therefore, the extended Lagrangian of the system is written as follows:

$$\begin{aligned} \mathcal{L}_{\text{hybrid}}^{\text{charge}} = & \frac{1}{2} \sum_{i=1}^N m_i \dot{\vec{r}}_i^2 + \frac{1}{2} \sum_{i=1}^N m_s (\dot{q}_{i,\text{aux}}^s)^2 \\ & + \frac{1}{2} \sum_{i=1}^N m_t (\dot{q}_{i,\text{aux}}^t)^2 - U(\vec{r}^N, q^N) - \frac{1}{2} \omega^2 \\ & \sum_{i=1}^N m_s (q_{i,\text{aux}}^s - q_{i,\text{SCF}}^s)^2 - \frac{1}{2} \omega^2 \\ & \sum_{i=1}^N m_t (q_{i,\text{aux}}^t - q_{i,\text{SCF}}^t)^2 \end{aligned} \quad (19)$$

where  $\vec{r}_i$  is the position vector of atom  $i$ ,  $U$  is the ReaxFF potential energy, the auxiliary charges,  $q_{i,\text{aux}}^s$  and  $q_{i,\text{aux}}^t$  evolve in time subject to a harmonic potential around the real charges,  $q_{i,\text{SCF}}^s$  and  $q_{i,\text{SCF}}^t$ , and  $m_i$ ,  $m_s$ , and  $m_t$  are the masses of atom  $i$ , s's, and t's, respectively. The above extended Lagrangian yields unstable dynamics due to accumulation of numerical error from insufficient convergence of the SCF, which manifests as increased kinetic energy of the auxiliary charges. Therefore, we apply Berendsen thermostats to the auxiliary charges, which stabilize their dynamics. In Figure 8a, we plot the energy as a function of time for the FeOH<sub>3</sub> system, comparing the original CG method with iEL-SCF using various convergence thresholds. It is evident that the iEL-SCF allows stable dynamics even at high convergence tolerance thresholds of  $5e^{-4}$  for the  $q_{\text{aux}}^s$  and  $e^{-4}$  for the  $q_{\text{aux}}^t$ . Furthermore, it is shown in Figure 8b that the number of SCF cycles with iEL-SCF can be reduced to around a third of the number of SCF cycles using CG at  $10^{-8}$ .

While the number of iterations to solve the EEM equations can be greatly reduced by iEL-SCF methods, it would be more desirable to eliminate iterations altogether by incorporating stochastic-XLMD-like approaches. In this direction, Tan et al.<sup>64</sup> introduced the SC-XLMD (stochastic constrained XLMD) approach, which is a re-formulation of a previous iteration-free scheme, stochastic-XLMD.<sup>51</sup> Since stochastic-XLMD was originally designed for polarizable models, the key ingredient here is employing the constraint of the invariance of the total charge. Therefore, both the charges  $\mathbf{q} = (q_1, \dots, q_N)$  and the chemical potential  $\mu$  are considered latent positions  $\mathbf{l} = (\mathbf{q}, \mu)$ , with latent momenta  $\mathbf{p}_l = (\mathbf{p}_q, p_\mu)$  and latent mass  $M_l = m_q I_n m_\mu$ .

The atomic and latent variables evolve according to the following extended Hamiltonian:

$$\begin{aligned} H_{\text{ext}}(\mathbf{r}, \mathbf{p}, \mathbf{l}, \mathbf{p}_l) = & \frac{1}{2} \mathbf{p}^T \mathbf{M}^{-1} \mathbf{p} + \frac{1}{2} \mathbf{p}_l^T \mathbf{M}_l^{-1} \mathbf{p}_l + U(r) \\ & + \frac{1}{2} \mathbf{l}^T \begin{pmatrix} \mathbf{J}(\mathbf{r}) & -1 \\ -1 & 0 \end{pmatrix} - \begin{pmatrix} -\chi \\ 0 \end{pmatrix}^T \mathbf{l} \end{aligned} \quad (20)$$

Similar to the iEL-SCF method, the latent variables are further thermostatted with a Langevin thermostat. The appropriate thermostat coupling constant,  $\gamma$ , however, should be determined from preliminary tests, where the thermostatting can both control the latent temperature and obtain sufficient energy conservation. Figure 8c,d presents the effect of the thermostat coupling parameter on the energy conservation and temperature of the latent variables, respectively. It is shown that while increasing the thermostat coupling parameter results in poorer energy conservation (Figure 8c), it allows stabilization of the temperature of the latent variables (Figure 8d). Therefore, a small thermostat coupling should be used. Both the iEL-SCF and the SC-XLMD methods have recently been added to the LAMMPS computational program.

## CONCLUSION AND FUTURE DIRECTIONS

We have summarized recent efforts to improve the accuracy, transferability, and efficiency of bond order reactive force fields as exemplified by models such as ReaxFF. Here we also suggest possible future directions for reactive force fields in general and bond order methods more specifically.

As the rate limiting step of energy and force evaluation is the SCF solution of the charge rearrangements as molecules undergo reactive steps, much progress has been made through extended Lagrangian schemes for solving charge equilibration. The iEL-SCF method has been shown to substantially reduce the number of SCF iterations by 40–80% while allowing stable dynamics at lower convergence tolerance thresholds.<sup>54</sup> In addition, the SAI preconditioners have been shown to provide a significant improvement with respect to the Jacobi preconditioner that is currently utilized in LAMMPS. Future work can assess whether combining iEL-SCF or SC-XLMD with SAI preconditioners can further enhance the efficiency of the charge equilibration methods. But with careful formulation of thermostatting parameters, the SC-XLMD method eliminates the requirement for solving a self-consistent solution of charge equilibration altogether and is most economical<sup>64,51</sup> and is now available in LAMMPS for others to evaluate. All of these approaches are also extensible to the more accurate ACKS2 scheme in lieu of using any of the related EEM or Qeq methods.

Perhaps one of the most important areas of progress in regards accuracy is using models such as eReaxFF (which replaces EEM with ACKS2) and core–shell models such as C-GeM,<sup>53,60</sup> both of which more explicitly account for electrons and electronic rearrangements. Together they have overcome some of the original failings of EEM, now allowing for reactive molecules to correctly dissociate into integer charge fragments so that redox reactions are better described and there is no longer any unphysical long-range charge transfer, while also accounting for out-of-plane polarization while mitigating metal overpolarization. A unique feature of eReaxFF is that it incorporates modified bond order terms that couple the charge state of an atom with its chemical activity. Recent applications of the eReaxFF have demonstrated that pairing every atom with an electron in a quasi-Drude type model is showing promising

results. Current research is working to extend the applications of the “quasi-Drude” eReaxFF to other systems such as water and graphite. While the ACKS2 method comes at the expense of greater computational cost, again it could be extended to using the extended Lagrangian schemes such as iEL/SCF and matrix preconditioners or SC-XLMD for accelerating its computational performance.

C-GeM has also been shown to provide a completely different alternative to EEM or ACKS2, yields the same benefits of eReaxFF, and is further extensible to electron transfer processes and accounting for electrostatic features such as sigma holes. Current research is focused on extending C-GeM to biomolecules and drug-like small molecule compounds through force field atom-typing that significantly enhances the accuracy of C-GeM relative to ab initio charge schemes for electrostatic potentials. Future research will work on implementing the atom-typed C-GeM in nonreactive force fields for molecular dynamics, which will benefit from high accuracy and a unified framework for treating permanent electrostatics, polarization, and charge transfer. Another research direction is to combine C-GeM with eReaxFF, thus eliminating the requirement for solving the ACKS2 equations. Based on the flexibility of LAMMPS, recent methods for embedding the ReaxFF/C-GeM model within a nonreactive force field allow for an extended environment for which reactivity can be represented in a localized region just like other QM/MM approaches. To date the hybrid approach has only been applied for systems where the nonreactive and reactive region interact through nonbonded interactions. Future research should extend the hybrid approach to include also a covalently bonded interface between the reactive and nonreactive regions. In addition, while there has been preliminary indications that show that ACKS2 and C-GeM provide a more accurate reactive force field, more work should be devoted to assessing when EEM is sufficient and when switching to the more accurate models is worth the development efforts of reparametrizing. To conclude, bond order reactive force fields such as ReaxFF are one of few methods available for chemists to computationally account for chemical reactivity in large scale simulations. As such, we believe the developments outlined here should realize new applications of reactive models in many areas of chemistry.

## AUTHOR INFORMATION

### Corresponding Author

Teresa Head-Gordon – Pitzer Center for Theoretical Chemistry, Department of Chemistry and Departments of Bioengineering and Chemical and Biomolecular Engineering, University of California, Berkeley, California 94720, United States; Chemical Sciences Division, Lawrence Berkeley National Laboratory, Berkeley, California 94720, United States; [ORCID](https://orcid.org/0000-0003-0025-8987); Email: [thg@berkeley.edu](mailto:thg@berkeley.edu)

### Authors

Itai Leven – Pitzer Center for Theoretical Chemistry, Department of Chemistry, University of California, Berkeley, California 94720, United States; Chemical Sciences Division, Lawrence Berkeley National Laboratory, Berkeley, California 94720, United States  
Hongxia Hao – Pitzer Center for Theoretical Chemistry, Department of Chemistry, University of California, Berkeley, California 94720, United States; Chemical Sciences Division,

Lawrence Berkeley National Laboratory, Berkeley, California 94720, United States

Songchen Tan – College of Chemistry and Molecular Engineering, Peking University, Beijing 100871, China

Xingyi Guan – Pitzer Center for Theoretical Chemistry, Department of Chemistry, University of California, Berkeley, California 94720, United States; Chemical Sciences Division, Lawrence Berkeley National Laboratory, Berkeley, California 94720, United States

Katheryn A. Penrod – Department of Mechanical Engineering, Chemical Engineering, Engineering Science and Mechanics, Chemistry, Materials Science and Engineering, Penn State University, University Park, Pennsylvania 16802, United States

Dooman Akbarian – Department of Mechanical Engineering, Chemical Engineering, Engineering Science and Mechanics, Chemistry, Materials Science and Engineering, Penn State University, University Park, Pennsylvania 16802, United States

Benjamin Evangelisti – Department of Mechanical Engineering, Chemical Engineering, Engineering Science and Mechanics, Chemistry, Materials Science and Engineering, Penn State University, University Park, Pennsylvania 16802, United States

Md Jamil Hossain – Department of Mechanical Engineering, Chemical Engineering, Engineering Science and Mechanics, Chemistry, Materials Science and Engineering, Penn State University, University Park, Pennsylvania 16802, United States; [ORCID](https://orcid.org/0000-0002-8737-2821)

Md Mahbubul Islam – Department of Mechanical Engineering, Wayne State University, Detroit, Michigan 48202, United States; [ORCID](https://orcid.org/0000-0003-4584-2204)

Jason P. Koski – Sandia National Laboratories, Albuquerque, New Mexico 87185-1315, United States; [ORCID](https://orcid.org/0000-0001-5740-8259)

Stan Moore – Sandia National Laboratories, Albuquerque, New Mexico 87185-1315, United States

Hasan Metin Aktulga – Department of Computer Science and Engineering, Michigan State University, East Lansing, Michigan 48824, United States

Adri C. T. van Duin – Department of Mechanical Engineering, Chemical Engineering, Engineering Science and Mechanics, Chemistry, Materials Science and Engineering, Penn State University, University Park, Pennsylvania 16802, United States

Complete contact information is available at:  
<https://pubs.acs.org/10.1021/acs.jctc.1c00118>

### Notes

The authors declare no competing financial interest.

## ACKNOWLEDGMENTS

This work was supported by the National Science Foundation under Grant CHE-1955643 (I.L. and T.H.-G.). We also acknowledge the CPIMS program by the Director, Office of Science, Office of Basic Energy Sciences, Chemical Sciences Division of the U.S. Department of Energy, under Contract No. DE-AC02-05CH11231 for the reverse micelle study (X.G., H.H., I.L., T.H.-G.). S.T. thanks the University of California Education Aboard Program (UCEAP) for financial and visa support. M.A. was supported in part by a Strategic Partnership Grant from the Michigan State University Foundation, an NSF

CDS&E grant (award number 1807622), and an NIH grant (award number GM130641). A.C.T.v.D., K.A.P., D.A.B.E., and Md.J.H. were supported by NSF CDS&E grant no. 1807622, the U.S. Army Research Laboratory through the Collaborative Research Alliance for Multi-Scale Multidisciplinary Modeling of Electronic Materials (MSME) under Cooperative Agreement No. W911NF-12-2-0023, and NSF NRT Grant No. DGE-1449785. This work used computational resources provided by the Institute for Cyber-Enabled Research at Michigan State University and the National Energy Research Scientific Computing Center (NERSC), a U.S. Department of Energy Office of Science User Facility operated under Contract No. DE-AC02-05CH11231. This project was supported by LDRD project 218473. Sandia National Laboratories is a multimission laboratory managed and operated by National Technology and Engineering Solutions of Sandia, LLC, a wholly owned subsidiary of Honeywell International, Inc., for the US Department of Energy's National Nuclear Security Administration under contract DE-NA0003525. This work describes objective technical results and analysis. Any subjective views or opinions that might be expressed in the work do not necessarily represent the views of the US Department of Energy or the United States Government.

## ■ REFERENCES

- (1) Gasteiger, J.; Marsili, M. A new model for calculating atomic charges in molecules. *Tetrahedron Lett.* **1978**, *19*, 3181–3184.
- (2) Parr, R. G.; Pearson, R. G. J. Absolute hardness: companion parameter to absolute electronegativity. *J. Am. Chem. Soc.* **1983**, *105*, 7512–7516.
- (3) Mortier, W. J.; Van Geuchten, K.; Gasteiger, J. Electronegativity equalization: application and parametrization. *J. Am. Chem. Soc.* **1985**, *107*, 829–835.
- (4) Mortier, W. J.; Ghosh, S. K.; Shankar, S. Electronegativity Equalization Method for the Calculation of Atomic Charges in Molecules. *J. Am. Chem. Soc.* **1986**, *108*, 4315–4320.
- (5) Tersoff, J. New Empirical-Approach for the Structure and Energy of Covalent Systems. *Phys. Rev. B: Condens. Matter Mater. Phys.* **1988**, *37*, 6991–7000.
- (6) Brenner, D. W. Empirical Potential for Hydrocarbons for Use in Simulating the Chemical Vapor-Deposition of Diamond Films. *Phys. Rev. B: Condens. Matter Mater. Phys.* **1990**, *42*, 9458–9471.
- (7) Rappé, A. K.; Goddard, W. A. Charge equilibration for molecular dynamics simulations. *J. Phys. Chem.* **1991**, *95*, 3358–3363.
- (8) Plimpton, S. Fast Parallel Algorithms for Short-Range Molecular Dynamics. *J. Comput. Phys.* **1995**, *117*, 1–19.
- (9) Chelli, R.; Proccaci, P.; Righini, R.; Califano, S. Electrical response in chemical potential equalization schemes. *J. Chem. Phys.* **1999**, *111*, 8569–8575.
- (10) Jakalian, A.; Bush, B. L.; Jack, D. B.; Bayly, C. I. Fast, efficient generation of highquality atomic charges. AM1-BCC model: I. Method. *J. Comput. Chem.* **2000**, *21*, 132–146.
- (11) Van Duin, A. C. T.; Dasgupta, S.; Lorant, F.; Goddard, W. A. ReaxFF: A Reactive Force Field for Hydrocarbons. *J. Phys. Chem. A* **2001**, *105*, 9396–9409.
- (12) Wang, J.; Wang, W.; Kollman, P. A.; Case, D. A. Automatic atom type and bond type in molecular mechanical calulations. *J. Mol. Graph Model* **2006**, *25*, 247–260.
- (13) Brenner, D. W.; Shenderova, O. A.; Harrison, J. A.; Stuart, S. J.; Ni, B.; Sinnott, S. B. A second-generation reactive empirical bond order (REBO) potential energy expression for hydrocarbons. *J. Phys.: Condens. Matter* **2002**, *14*, 783–802.
- (14) Strachan, A.; Kober, E. M.; Van Duin, A. C.; Oxgaard, J.; Goddard, W. A. Thermal decomposition of RDX from reactive molecular dynamics. *J. Chem. Phys.* **2005**, *122*, 054502.
- (15) Wang, J.; Wang, W.; Kollman, P. A.; Case, D. A. Automatic atom type and bond type perception in molecular mechanical calculations. *J. Mol. Graphics Modell.* **2006**, *25*, 247–260.
- (16) Chen, J.; Martínez, T. J. QTPIE: Charge transfer with polarization current equalization. A fluctuating charge model with correct asymptotics. *Chem. Phys. Lett.* **2007**, *438*, 315–320.
- (17) Mathieu, D. Split charge equilibration method with correct dissociation limits. *J. Chem. Phys.* **2007**, *127*, 224103.
- (18) Yu, J.; Sinnott, S. B.; Phillipot, S. R. Charge optimized many-body potential for the SiSiO<sub>2</sub> system. *Phys. Rev. B: Condens. Matter Mater. Phys.* **2007**, *75*, 085311.
- (19) Chenoweth, K.; van Duin, A. C. T.; Goddard, W. A. ReaxFF Reactive Force Field for Molecular Dynamics Simulations of Hydrocarbon Oxidation. *J. Phys. Chem. A* **2008**, *112*, 1040–1053.
- (20) McNeill, V.; Yatavelli, R.; Thornton, J.; Stipe, C.; Landgrebe, O. Heterogeneous OH oxidation of palmitic acid in single component and internally mixed aerosol particles: vaporization and the role of particle phase. *Atmos. Chem. Phys.* **2008**, *8*, 5465.
- (21) Aktulga, H.; Fogarty, J.; Pandit, S.; Gramma, A. Parallel reactive molecular dynamics: Numerical methods and algorithmic techniques. *Parallel Computing* **2012**, *38*, 245–259.
- (22) Aktulga, H. M.; Pandit, S. A.; van Duin, A. C. T.; Gramma, A. Y. Reactive Molecular Dynamics: Numerical Methods and Algorithmic Techniques. *SIAM J. Sci. Comput.* **2012**, *34*, C1–C23.
- (23) Stevanović, V.; Lany, S.; Zhang, X.; Zunger, A. Correcting density functional theory for accurate predictions of compound enthalpies of formation: Fitted elemental-phase reference energies. *Phys. Rev. B: Condens. Matter Mater. Phys.* **2012**, *85*, 115104.
- (24) Monti, S.; Corozzi, A.; Fristrup, P.; Joshi, K. L.; Shin, Y. K.; Oelschlaeger, P.; Van Duin, A. C.; Barone, V. Exploring the conformational and reactive dynamics of biomolecules in solution using an extended version of the glycine reactive force field. *Phys. Chem. Chem. Phys.* **2013**, *15*, 15062–15077.
- (25) Verstraelen, T.; Ayers, P. W.; Van Speybroeck, V.; Waroquier, M. ACKS2: Atom-condensed Kohn-Sham DFT approximated to second order. *J. Chem. Phys.* **2013**, *138*, 074108.
- (26) Carter Edwards, H.; Trott, C. R.; Sunderland, D. Kokkos: Enabling manycore performance portability through polymorphic memory access patterns. *J. Parallel and Distributed Computing* **2014**, *74*, 3202–3216.
- (27) Ghysels, P.; Vanroose, W. Hiding global synchronization latency in the preconditioned conjugate gradient algorithm. *Parallel Computing* **2014**, *40*, 224–238.
- (28) Gramma, A.; Aktulga, H. M.; Kyłasa, S. B. PuReMD, *Purdue Reactive Molecular Dynamics package*, 2014, <https://www.cs.purdue.edu/puremd>, Accessed on June 8, 2016.
- (29) Himmetoglu, B.; Floris, A.; De Gironcoli, S.; Cococcioni, M. Hubbard-corrected DFT energy functionals: The LDA+ U description of correlated systems. *Int. J. Quantum Chem.* **2014**, *114*, 14–49.
- (30) Mardirossian, N.; Head-Gordon, M. B97X-V: A 10-parameter, range-separated hybrid, generalized gradient approximation density functional with nonlocal correlation, designed by a survival-of-the-fittest strategy. *Phys. Chem. Chem. Phys.* **2014**, *16*, 9904–9924.
- (31) Shan, T. R.; Van Duin, A. C.; Thompson, A. P. Development of a ReaxFF reactive force field for ammonium nitrate and application to shock compression and thermal decomposition. *J. Phys. Chem. A* **2014**, *118*, 1469–1478.
- (32) Verlackt, C. C.; Neyts, E. C.; Jacob, T.; Fantauzzi, D.; Golkaram, M.; Shin, Y. K.; Van Duin, A. C.; Bogaerts, A. Atomic-scale insight into the interactions between hydroxyl radicals and DNA in solution using the ReaxFF reactive force field. *New J. Phys.* **2015**, *17*, 103005.
- (33) Boes, J. R.; Groenenboom, M. C.; Keith, J. A.; Kitchin, J. R. Neural network and ReaxFF comparison for Au properties. *Int. J. Quantum Chem.* **2016**, *116*, 979–987.
- (34) Hjertenes, E.; Nguyen, A. Q.; Koch, H. A ReaxFF force field for sodium intrusion in graphitic cathodes. *Phys. Chem. Chem. Phys.* **2016**, *18*, 31431–31440.
- (35) Islam, M. M.; Kolesov, G.; Verstraelen, T.; Kaxiras, E.; Van Duin, A. C. EReaxFF: A Pseudoclassical Treatment of Explicit Electrons

- within Reactive Force Field Simulations. *J. Chem. Theory Comput.* **2016**, *12*, 3463–3472.
- (36) Islam, M. M.; van Duin, A. C. T. Reductive Decomposition Reactions of Ethylene Carbonate by Explicit Electron Transfer from Lithium: An eReaxFF Molecular Dynamics Study. *J. Phys. Chem. C* **2016**, *120*, 27128–27134.
- (37) Kylasa, S. B.; Aktulga, H. M.; Grama, A. Y. Reactive molecular dynamics on massively parallel heterogeneous architectures. *IEEE Transactions on Parallel and Distributed Systems* **2017**, *28*, 202–214.
- (38) Müller, J.; Hartke, B. reaxFF Reactive Force Field for Disulfide Mechanochemistry, Fitted to Multireference ab Initio Data. *J. Chem. Theory Comput.* **2016**, *12*, 3913–3925.
- (39) O’Hearn, K. A.; Aktulga, H. M. *Proceedings of the 7th Workshop on Latest Advances in Scalable Algorithms for Large-Scale Systems (ScalA)*; IEEE Press, 2016; pp 9–16.
- (40) Psolfogiannakis, G.; Van Duin, A. C. Development of a ReaxFF reactive force field for Si/Ge/H systems and application to atomic hydrogen bombardment of Si, Ge, and SiGe (100) surfaces. *Surf. Sci.* **2016**, *646*, 253–260.
- (41) Senftle, T. P.; Hong, S.; Islam, M. M.; Kylasa, S. B.; Zheng, Y.; Shin, Y. K.; Junkermeier, C.; Engel-Herbert, R.; Janik, M. J.; Aktulga, H. M.; Verstraelen, T.; Grama, A.; van Duin, A. C. T. The ReaxFF reactive force-field: development, applications and future directions. *npj Computational Materials* **2016**, *2*, 15011.
- (42) Ashraf, C.; van Duin, A. C. Extension of the ReaxFF Combustion Force Field toward Syngas Combustion and Initial Oxidation Kinetics. *J. Phys. Chem. A* **2017**, *121*, 1051–1068.
- (43) Giberti, F.; Hassanali, A. A. The excess proton at the air-water interface: The role of instantaneous liquid interfaces. *J. Chem. Phys.* **2017**, *146*, 244703.
- (44) Qiu, Y.; Odendahl, N.; Hudait, A.; Mason, R.; Bertram, A. K.; Paesani, F.; DeMott, P. J.; Molinero, V. Ice nucleation efficiency of hydroxylated organic surfaces is controlled by their structural fluctuations and mismatch to ice. *J. Am. Chem. Soc.* **2017**, *139*, 3052–3064.
- (45) Wang, N.; Peng, J.; Pang, A.; He, T.; Du, F.; Jaramillo-Botero, A. Thermodynamic Simulation of the RDX-Aluminum Interface Using ReaxFF Molecular Dynamics. *J. Phys. Chem. C* **2017**, *121*, 14597–14610.
- (46) Yun, K. S.; Pai, S. J.; Yeo, B. C.; Lee, K. R.; Kim, S. J.; Han, S. S. Simulation Protocol for Prediction of a Solid-Electrolyte Interphase on the Silicon-based Anodes of a Lithium-Ion Battery: ReaxFF Reactive Force Field. *J. Phys. Chem. Lett.* **2017**, *8*, 2812–2818.
- (47) Lu, K.; He, Y.; Huo, C. F.; Guo, W. P.; Peng, Q.; Yang, Y.; Li, Y. W.; Wen, X. D. Developing ReaxFF to Visit CO Adsorption and Dissociation on Iron Surfaces. *J. Phys. Chem. C* **2018**, *122*, 27582–27589.
- (48) Trnka, T.; Tvaroška, I.; Koča, J. Automated Training of ReaxFF Reactive Force Fields for Energetics of Enzymatic Reactions. *J. Chem. Theory Comput.* **2018**, *14*, 291–302.
- (49) Akbarian, D.; Yilmaz, D. E.; Cao, Y.; Ganesh, P.; Dabo, I.; Munro, J.; Van Ginneken, R.; Van Duin, A. C. Understanding the influence of defects and surface chemistry on ferroelectric switching: A ReaxFF investigation of BaTiO<sub>3</sub>. *Phys. Chem. Chem. Phys.* **2019**, *21*, 18240–18249.
- (50) Aktulga, H. M.; Knight, C.; Coffman, P.; O’Hearn, K. A.; Shan, T.-R.; Jiang, W. Optimizing the performance of reactive molecular dynamics simulations for many-core architectures. *Int. J. High Perf. Comp. App.* **2019**, *33*, 304–321.
- (51) An, D.; Cheng, S. Y.; Head-Gordon, T.; Lin, L.; Lu, J. Convergence of Stochastic-extended Lagrangian molecular dynamics method for polarizable force field simulation. *J. Comput. Phys.* **2021**, *110338*.
- (52) Furman, D.; Wales, D. J. Transforming the Accuracy and Numerical Stability of ReaxFF Reactive Force Fields. *J. Phys. Chem. Lett.* **2019**, *10*, 7215–7223.
- (53) Leven, I.; Head-Gordon, T. C-GeM: Coarse-Grained Electron Model for Predicting the Electrostatic Potential in Molecules. *J. Phys. Chem. Lett.* **2019**, *10*, 6820–6826.
- (54) Leven, I.; Head-Gordon, T. Inertial extended-Lagrangian scheme for solving charge equilibration models. *Phys. Chem. Chem. Phys.* **2019**, *21*, 18652–18659.
- (55) O’Hearn, K. A.; Alperen, A.; Aktulga, H. M. In *Proceedings of the ACM Int. Conference on Supercomputing*; Association for Computing Machinery: New York, 2019; pp 150–159.
- (56) Bertels, L. W.; Newcomb, L. B.; Alaghemandi, M.; Green, J. R.; Head-Gordon, M. Benchmarking the Performance of the ReaxFF Reactive Force Field on Hydrogen Combustion Systems. *J. Phys. Chem. A* **2020**, *124*, 5631–5645.
- (57) Evangelisti, B.; Fichthorn, K. A.; Van Duin, A. C. T. Development and initial applications of an e-ReaxFF description of Ag nanoclusters. *J. Chem. Phys.* **2020**, *153*, 104106.
- (58) Furman, D.; Wales, D. J. A well-behaved theoretical framework for ReaxFF reactive force fields. *J. Chem. Phys.* **2020**, *153*, 021102.
- (59) Hossain, M. J.; Pawar, G.; Liaw, B.; Gering, K. L.; Dufek, E. J.; Van Duin, A. C. Lithium-electrolyte solvation and reaction in the electrolyte of a lithium ion battery: A ReaxFF reactive force field study. *J. Chem. Phys.* **2020**, *152*, 184301.
- (60) Leven, I.; Hao, H.; Das, A. K.; Head-Gordon, T. A Reactive Force Field with Coarse-Grained Electrons for Liquid Water. *J. Phys. Chem. Lett.* **2020**, *11*, 9240–9247.
- (61) O’Hearn, K. A.; Alperen, A.; Aktulga, H. M. Fast Solvers for Charge Distribution Models on Shared Memory Platforms. *SIAM J. Sci. Comput.* **2020**, *42*, C1–C22.
- (62) O’Hearn, K. A.; Swift, M. W.; Liu, J.; Magoulas, I.; Piecuch, P.; van Duin, A. C.; Aktulga, H. M.; Qi, Y. Optimization of the Reax force field for the lithium-oxygen system using a high fidelity charge model. *J. Chem. Phys.* **2020**, *153*, 084107.
- (63) Rahnamoun, A.; Kaymak, M. C.; Manathunga, M.; Götz, A. W.; Van Duin, A. C.; Merz, K. M., Jr.; Aktulga, H. M. ReaxFF/AMBERIA Framework for Hybrid Reactive/Nonreactive Force Field Molecular Dynamics Simulations. *J. Chem. Theory Comput.* **2020**, *16*, 7645–7654.
- (64) Tan, S.; Leven, I.; An, D.; Lin, L.; Head-Gordon, T. Stochastic Constrained Extended System Dynamics for Solving Charge Equilibration Models. *J. Chem. Theory Comput.* **2020**, *16*, 5991–5998.
- (65) Adams, E.; Hao, H.; Leven, I.; Rüttermann, M.; Wirtz, H.; Havenith, M.; Head-Gordon, T. Proton Traffic Jam: Effect of Nanoconfinement and Acid Concentration on Proton Hopping Mechanism. *Angewandte Chemie* **2021**, submitted for publication.
- (66) Akbarian, D.; Ganeshan, K.; Woodward, W. H. H.; Moore, J.; van Duin, A. C. T. Atomistic-scale insight into the polyethylene electrical breakdown: An eReaxFF molecular dynamics study. *J. Chem. Phys.* **2021**, *154*, 024904.